Finite Temporal Support Pulses for em Excitation

Lager, Ioan; van Berkel, Sven

DOI
10.1109/LAWP.2017.2662205

Publication date
2017

Document Version
Accepted author manuscript

Published in
IEEE Antennas and Wireless Propagation Letters

Finite Temporal Support Pulses for EM Excitation

Ioan E. Lager, *Senior Member, IEEE*, and Sven L. van Berkel, *Student Member, IEEE*

***Abstract*—A new family of pulses is introduced. It consists of a windowed-power (WP), unipolar prototype, a unicycle, and a pulse with almost rectangular spectral diagram. These pulses have finite temporal support, controlled continuity at onset and end, and are tailored via simple design rules. The WP prototype has a very low spectral leakage. The WP monocycle's effectiveness as excitation in computational schemes is demonstrated via numerical experiments. Its signature is also shown to practically overlap one generated by readily available circuitry. The WP pulses are opportune as excitation in electromagnetic analysis, for time-windowing purposes, and for feeding pulsed-field or timed antenna arrays.**

***Index Terms*—Antennas, pulse generation, time-domain (TD) analysis.**

I. Introduction

THE opportunity of causality and controlled differentiability of model pulses used as excitation in electromagnetic (EM) analysis was discussed in [1]. That paper introduced a family of causal pulses derived from the power exponential (PE) unipolar prototype. However, EM simulations can largely benefit from excitations with finite temporal support (see Section V-A). PE pulses lack this feature (their tail extends to infinity), and pulses combining finite temporal support, controlled differentiability and shape control via few parameters are then needed. By starting from a *windowed-power* (WP) prototype, this letter introduces a novel family of model pulses providing all these qualities. Following [2], the family is endowed with a pulse with almost flat spectral contents in a prescribed bandwidth. This feature is similar to the band limitation offered by, for example, the approximate prolate wave function [3], but the WP-based pulse has the advantage of being time-windowed.

Temporal boundedness is also an important enabler for timed array antennas [4]. Inspired by (mechanically) switching ON and OFF a single-tone feeding signal, such antenna (models) use rectangular time-windowed sinusoidal excitations. Nonetheless, the far-field EM field radiated by antennas is *at least* the time-derivative of the feeding signal's signature [5] (the received signal in a loop-to-loop transfer being the third-order time-derivative of the feeding current [6]). Consequently, ON/OFF switched sine feeding signals render the radiated EM field *at least* discontinuous. Conversely, imposing the continuity of the radiated EM field requires the feeding signal to be discontinuous. None of these situations is physical. The WP unipolar prototype resolves this issue: It combines time-windowing with controlled differentiability. Moreover, it offers exceptionally low spectral leakage (SpL), an essential figure of merit of any apodization function [7, p. 55].

Manuscript received November 17, 2016; revised January 3, 2017; accepted January 10, 2017. Date of publication February 1, 2017; date of current version June 19, 2017.

The authors are with the Faculty of Electrical Engineering, Mathematics and Computer Science, Delft University of Technology, CD Delft 2628, The Netherlands (e-mail: i.e.lager@tudelft.nl; s.l.vanberkel@tudelft.nl).

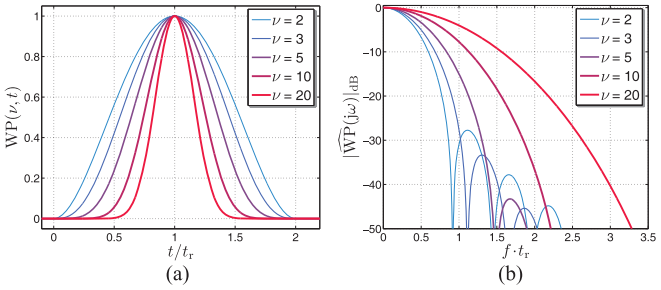

Fig. 1. WP model pulse. (a) Temporal signature. (b) Spectral diagram.

This letter will first introduce the WP unipolar prototype. The WP monocycle and a pulse with almost rectangular spectral diagram will be then derived from it. The WP monocycle's adequacy will be proven via illustrative numerical experiments and by demonstrating its physical reproducibility.

II. WP Unipolar Prototype

The WP family of model pulses is constructed by starting from the *WP unipolar prototype* originally introduced in [8]

$$\mathrm{WP}(\nu,t) = t'^{\nu}(2-t')^{\nu}H(t')H(2-t') \tag{1}$$

where $\nu = 2, 3, 4, \ldots$, is the pulse rising power, t the time coordinate, $t' = t/t_r$, with $t_r > 0$ being the pulse rise-time (the time between onset and the instant when the pulse peaks), and $H(\cdot)$ the Heaviside unit step function. This pulse has a *finite temporal support* $2t_r$, being implicitly causal. The support of its first ν time-derivatives is also $2t_r$. The pulse and its first $\nu-1$ time-derivatives are continuous at both onset and end—the choice $\nu \geqslant 2$ ensures this type of continuity at least for $\partial_t \mathrm{WP}(\nu,t)$. The WP prototype is normalized to unity.

The Fourier transform of $\mathrm{WP}(\nu,t)$ can be shown to be

$$\widehat{\mathrm{WP}}(\nu,\mathrm{j}\omega) = \exp(-\mathrm{j}\omega t_r)\, t_r\, 2^{\nu}\nu!\sqrt{2\pi}\frac{J_{\nu+1/2}(\omega t_r)}{(\omega t_r)^{\nu+1/2}} \tag{2}$$

where $\omega = 2\pi f$, with f being the frequency, and $J_{n+1/2}$ is the Bessel function of the first kind and fractional order [9, Section 10.1]. Note that $|\widehat{\mathrm{WP}}(\mathrm{j}\omega)| = |\widehat{\mathrm{WP}}(-\mathrm{j}\omega)|$ since $\mathrm{WP}(\nu,t)$ is real. Examples of this pulse and the corresponding Bode diagrams are shown in Fig. 1. In it, $|\cdot|_{\mathrm{dB}}$ stands for $20\log_{10}(|\cdot|/|\cdot|_{\max})$.

The WP pulse is also favorable for time-windowing purposes. A key figure of merit to this end is the SpL [7, p. 55]

$$\mathrm{SpL} = P_{\mathrm{SL}}/P_{\mathrm{tot}} = (P_{\mathrm{tot}} - P_{\mathrm{ML}})/P_{\mathrm{tot}} \tag{3}$$

where P_{tot} is the total spectral power, P_{ML} is the power in the main lobe (ML), and P_{SL} is the total power in the sidelobes. For

TABLE I
SPL AND THE EXTENT OF THE SPECTRAL DIAGRAM'S ML FOR THE WP PULSE

ν	Spectral Leakage (SpL)	ML Limit
2	-28.7 dB	$0.92ft_r$
3	-35.1 dB	$1.11ft_r$
5	-45.9 dB	$1.49ft_r$
10	-68.4 dB	$2.39ft_r$
20	-106.4 dB	$4.13ft_r$

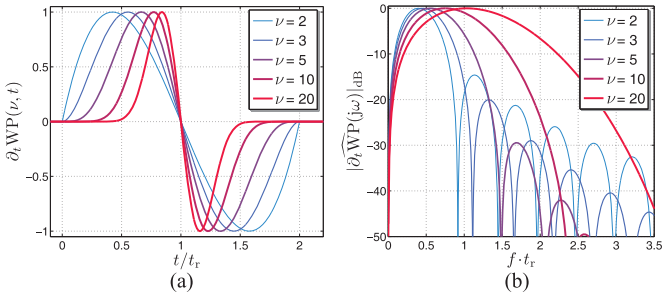

Fig. 2. ∂_tWP model pulse. (a) Temporal signature. (b) Spectral diagram.

$\mathrm{WP}(\nu,t)$, P_ML is evaluated from (2) by numerical integration while P_tot follows via Parseval's theorem as

$$P_\mathrm{tot} = \int_{t=0}^{2t_r} [\mathrm{WP}(\nu,t)]^2 \mathrm{d}t = t_r \frac{2^{4\nu+1}[(2\nu)!]^2}{(4\nu+1)!}. \tag{4}$$

The SpL and the ML limits are catalogued in Table I for the ν's in Fig. 1. The SpL is very low even for small ν's, this attesting the pulse's suitability for time-windowing purposes.

III. WP MONOCYCLE MODEL PULSE

Antenna systems are practically always fed by means of pulses with no dc component in their spectral diagram. Such a model pulse, denoted as *WP monocycle* (∂_tWP), is now constructed by taking the time-differential in (1)

$$\partial_t \mathrm{WP}(\nu,t) = N(\nu)2\nu(1-t')t'^{\nu-1}(2-t')^{\nu-1}H(t')H(2-t') \tag{5}$$

with $N(\nu) = t_r\,\nu^{-1}2^{-\nu}(\nu-1)^{1-\nu}(2\nu-1)^{\nu-1/2}$ ensuring a unit amplitude for the pulse. The WP monocycle has a zero-crossing at $t=t_r$ and has a maximum and a minimum at

$$t_{\mathrm{ex};\pm} = t_r\left[1 \pm (2\nu-1)^{-1/2}\right] \tag{6}$$

respectively. Its Fourier transform follows from (2), by multiplication by $\mathrm{j}\omega$. Examples of this pulse and the corresponding Bode diagrams are shown in Fig. 2. The spectral diagram's peak shifts to higher frequencies as ν increases. Fig. 3 illustrates the variation of the spectral diagram's peak and -3-dB limits for a wide range of ν values. This figure, in conjunction with the pulse width and its zero-crossing, provide a complete set of design rules for fitting the WP monocycle's parameters to the requirements of specific practical applications.

IV. WP MODULATED–SINC–COSINE MODEL PULSE

Numerical models often require excitations with a flat spectral diagram over a prescribed frequency range $f \in [f_l, f_h]$, $0 < f_l < f_h$, with center frequency $f_c = (f_l+f_h)/2$ and bandwidth $B = f_h - f_l$. The WP family is then supplemented with

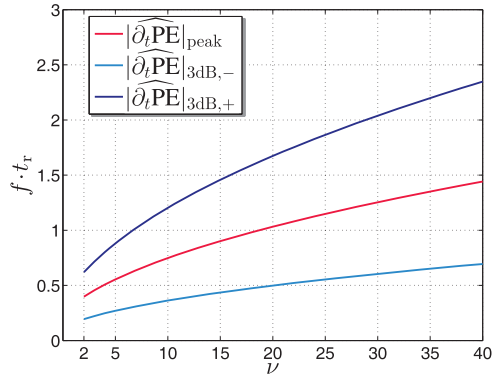

Fig. 3. Variation of the spectral diagram's peak and -3-dB limits as a function of ν for the ∂_tWP model pulse.

such a model pulse. In line with [2], $\mathrm{WP}(\nu,t)$ is used for time-windowing the *noncausal* function

$$G(t_0,t) = \mathrm{sinc}[B(t-t_0)]\cos[2\pi f_c(t-t_0)] \tag{7}$$

where $\mathrm{sinc}(x) \overset{\mathrm{def}}{=} \sin(\pi x)/(\pi x)$, for $x \in \mathbb{R}$, and $t_0 \geqslant 0$ is a time shift. The Fourier transform of (7) is

$$\hat{G}(t_0,\mathrm{j}\omega) = \frac{\exp(-\mathrm{j}\omega\, t_0)}{2B} \times \begin{cases} 1, & \text{for } \omega_l < |\omega| < \omega_h \\ 0, & \text{otherwise} \end{cases}. \tag{8}$$

Combining (1) and (7) then yields the *WP modulated–sinc–cosine (WPS-C) model pulse* defined as

$$\mathrm{WP_{S\text{-}C}}(\nu,B,t) = \mathrm{sinc}\,[B(t-t_r)]\cos\,[2\pi f_c(t-t_r)]\,\mathrm{WP}(\nu,t) \tag{9}$$

where t_r and B are interrelated via $t_r = K_\mathrm{sc}/B$, with $K_\mathrm{sc} = 1,2,3,\ldots$. The pulse's Fourier transform follows as:

$$\begin{aligned} \widehat{\mathrm{WP_{S\text{-}C}}}(\nu,B,\mathrm{j}\omega) &= \frac{1}{2\pi}\left[\widehat{\mathrm{WP}}(\nu,\mathrm{j}\omega) \overset{(\mathrm{j}\omega)}{*} \hat{G}(\mathrm{j}\omega)\right] \\ &= \frac{\exp(-\mathrm{j}\omega t_r)}{2B}\left[\mathcal{I}(-\omega_h,-\omega_l) + \mathcal{I}(\omega_l,\omega_h)\right] \end{aligned} \tag{10}$$

where $\overset{(\mathrm{j}\omega)}{*}$ denotes frequency convolution, $\omega_{l,h} = 2\pi f_{l,h}$ and

$$\mathcal{I}(\omega_\alpha,\omega_\beta) = \int_{\omega'=\omega+\omega_\alpha}^{\omega+\omega_\beta} \left[\exp(\mathrm{j}\omega' t_r)\widehat{\mathrm{WP}}(\nu,\mathrm{j}\omega')\right]\mathrm{d}\omega'. \tag{11}$$

The integral in (11) is amenable to numerical quadrature, the presented examples using the trapezoidal rule. Examples of the $\mathrm{WP_{S\text{-}C}}$ pulse and the corresponding Bode diagrams are shown in Fig. 4. The spectral behavior has the following features.

1) The spectral diagram approximates increasingly well a rectangular shape as K_sc increases, while the influence of ν on its shape is minimal.
2) $|\widehat{\mathrm{WP_{S\text{-}C}}}(\nu,B,\mathrm{j}\omega_{l,h})|^2 \approx 1/4$ for $K_\mathrm{sc} \geqslant 3$.
3) *Design rules:* By taking $K_\mathrm{sc} \geqslant 3$, t_r and f_c follow from the intended f_l and f_h, and ν can be chosen more or less arbitrarily for ensuring a certain pulse "smoothness."

These observations concur with those in [2, Section IV].

$\mathrm{WP_{S\text{-}C}}(\nu,B,t)$ also offers remarkably low SpL, as evidenced in Table II. This recommends it for band-limited frequency-domain studies performed via time-domain (TD) simulations.

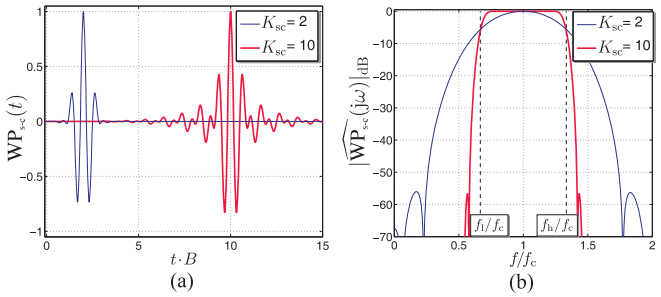

(a) (b)

Fig. 4. $\mathrm{WP}_{S\text{-}C}$ model pulse. (a) Temporal signature. (b) Spectral diagram.

TABLE II
SPL AND THE LIMITS OF THE SPECTRAL DIAGRAM'S ML FOR THE $\mathrm{WP}_{S\text{-}C}$ MODEL PULSE

K_{sc}	Spectral Leakage (SpL)	ML Limits
2	−61.1 dB	$0.23f/f_c$; $1.77f/f_c$
10	−69.3 dB	$0.58f/f_c$; $1.42f/f_c$

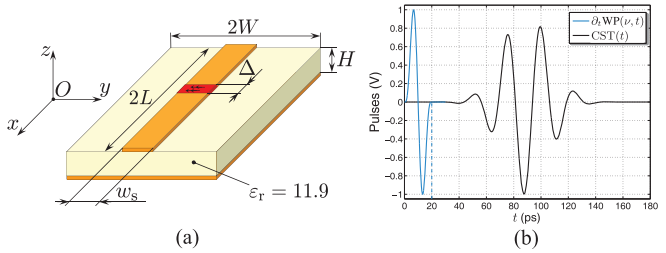

(a) (b)

Fig. 5. Explanatory for the CST simulations. (a) Examined infinitely long microstrip line; configuration parameters: $w_s = 100\,\mu$m, $\Delta = 0.7w_s$, and $H = 127\,\mu$m; the configuration is symmetric with respect to the $x = 0$ and $y = 0$ planes. (b) Signatures of the $\mathrm{CST}(t)$ and $\partial_t \mathrm{WP}(\nu, t)$ excitation pulses.

Nonetheless, the flat spectral diagram is obtained at the expense of enlarging the pulse's temporal support. As shown in Section V-A, this enlarges the computation times in the case of TD simulations. Finding an optimum balance between spectral flatness and computational effectiveness must be established on a case-by-case basis. The design rules given in this section provide the conducive instruments to this end.

V. PRACTICAL APPLICATIONS

The opportunity of the ∂_tWP pulse is now demonstrated by analyzing the impact of a ∂_tWP excitation on computational efficiency and the pulse's amenability to physical realization.

A. Time-Windowed EM Simulations

CST Microwave Studio has established itself in the antenna community as the *de facto* standard TD general-purpose EM simulation tool. In this section, it is shown via a simple yet illustrative example how a ∂_tWP excitation can massively improve the computational efficiency of this software. For emphasizing the effect of the advocated excitation, all simulations deliberately employ standard, basic runtime settings.

The investigated configuration [shown in Fig. 5(a)] concerns an infinitely extended, grounded microstrip line, with the strip and ground being perfectly conducting (PEC). For the chosen

TABLE III
CST MICROWAVE STUDIO SIMULATIONS RESULTS

L	Mesh Cells	Pulse	Term. Criterion	t_{SW}	t_{sim}	$\lvert\Delta_{\lvert S_{11}\rvert}\rvert$ Maximum
2 mm	400 000	∂_t WP	E.C.	45 ps	18 s	0.118%
2 mm	400 000	∂_t WP	T.W.	30 ps	**13 s**	0.025%
2 mm	400 000	CST	T.W.	180 ps	71 s	6.5%
10 mm	1 500 000	CST	T.W.	180 ps	308 s	0.023%
10 mm	1 500 000	CST	E.C.	270 ps	410 s	0.021%

$\varepsilon_r = 11.9$, the dimensions w_s and H ensure a 50-Ω characteristic impedance. The line is excited via a Δ-gap discrete port with a uniform field distribution over the gap's subtended area, its source impedance being of 50 Ω. In view of symmetry, only one quarter of the configuration is simulated. The boundary conditions follow from the symmetry at $x = 0$ and $y = 0$, are PEC type on the ground plane, and are perfectly matched layers (PML) type on all other boundaries. The line is examined for $f \in [20, 60]$ GHz where it is taken as nonradiative (no power is transferred into surface waves [10]). All injected energy should then reach the PML boundaries at $x = \pm L$ and leave the computational domain. However, the PML limitations cause some reflections. Eventually, after several reflections, practically all injected energy will leave the domain and the simulation can be stopped, this situation being termed as "energy convergence" (E.C.) termination. Prior to reaching the E.C. state, the boundary reflections cause spurious reflections at the Δ-gap feeding port. This study concerns exactly the reflection coefficient $|S_{11}(f)|$ at this port.

Simulations are first carried out for $L = 18$ mm and use a −30-dB E.C. termination. Two excitation pulses are employed: 1) the one constructed automatically by the package, hereafter denoted as $\mathrm{CST}(t)$; its length is $t_{p;\,\mathrm{CST}} = 180$ ps, and the pertaining results are henceforth taken as reference; 2) a ∂_tWP pulse with $\nu = 10$ and $t_r = 10$ ps; its length (including a zero tail) is $t_{p;\,\mathrm{WP}} = 30$ ps. The pulse signatures are shown in Fig. 5(b). The $|S_{11}(f)|$ decibel values obtained via the two excitations agree up to three decimals (see [8, Fig. 5]), this attesting the ∂_tWP pulse's suitability, but the computation time t_{sim} is 83% shorter in the case of the WP excitation.

A considerably higher computation time saving is achievable by exploiting the temporal finiteness of the WP monocycle. To this end, it is observed that no reflections from boundaries are sensed at the Δ-gap port if $L > L_{\mathrm{Rf}} = t_{\mathrm{SW}}\, c_0/\sqrt{\varepsilon_{r,\mathrm{eff}}}/2$, where t_{SW} is the simulation window, c_0 the EM wave speed in free space, and $\varepsilon_{r,\mathrm{eff}}$ the relative effective permittivity of the transmission line ($\sqrt{\varepsilon_{r,\mathrm{eff}}} = 2.85$ in this case). Simulations are stopped at t_{SW}, a strategy termed as "time-windowed" (T.W.) termination. Two reflections-free lengths $L_{\mathrm{WP}} = 2$ mm and $L_{\mathrm{CST}} = 10$ mm are determined by equating t_{SW} to $t_{p;\,\mathrm{WP}}$ and $t_{p;\,\mathrm{CST}}$, respectively, and adding a safety margin.

The effect of the various runtime parameters is examined in Table III and Fig. 6. The deviation of $|S_{11}(f)|$ (in dB) with respect to the reference $\mathrm{CST}(t)$/E.C. results is calculated as

$$\Delta_{|S_{11}|}(f) = \Big(|S_{11}(f)| - |S_{11}(f)|_{\mathrm{ref}}\Big)/|S_{11}(f)|_{\mathrm{ref}}. \qquad (12)$$

Fig. 6 shows the effect of the boundary reflections for the $\mathrm{CST}(t)$ excitation when $L = 2$ mm ($L \ll L_{\mathrm{Rf}}(t_{p;\,\mathrm{CST}})$). A minute effect is also visible for the ∂_tWP excitation with E.C. termination since $L < L_{\mathrm{Rf}}(t_{p;\,\mathrm{WP}})$. No boundary reflections

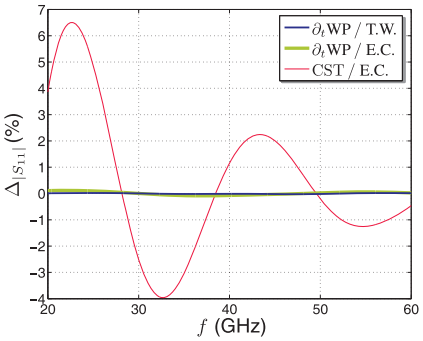

Fig. 6. Deviations with respect to the reference $|S_{11}|$ in the case of the computational domain with $L = 2$ mm.

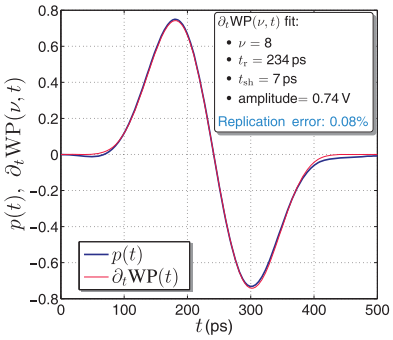

Fig. 7. Replication of the pulse signature $p(t)$ in [11, Fig. 10(b)] via a WP monocycle. The inset contains the pulse parameters and the replication error. The $p(t)$ signature is reproduced with written permission from the authors.

occur when using a ∂_tWP excitation in conjunction with T.W. termination, this combination yielding the shortest computation time, $t_{\mathrm{sim;WP}} = 13$ s. There is also no effect of boundary reflections when using a $\mathrm{CST}(t)$ excitation and $L = 10$ mm for both T.W. and E.C. terminations (see Table III). Nevertheless, the computation times are much larger, namely 308 s for T.W. ($23.7 \times t_{\mathrm{sim;WP}}$) and 410 s for E.C. ($31.5 \times t_{\mathrm{sim;WP}}$)! The massive computation time saving arising from using a ∂_tWP excitation with T.W. termination is conducive to ensuring the feasibility of optimization processes requiring numerous simulations. This is highly relevant for antenna design: Correlating the pulse length with the dimensions of the domain of computation may result in a reflections-free region where field quantities can be accurately evaluated.

B. Physical Reproducibility of the Model Pulses

An aspect of prime importance when designing (model) pulses is their physical reproducibility via (integrated) circuits. This study focuses on the WP monocycle due to its envisaged suitability as a feeding pulse for radio applications.

Let the pulse signature $p(t)$ in [11, Fig. 10(b)], the generating circuit being developed for ultrahigh data-rate transfer. $p(t)$ is now replicated via ∂_tWP (see Fig. 7). First, $t_{\mathrm{ex};\pm}$ in (6) are identified with the instants $t_{\mathrm{ex};\pm,p}$ when $p(t)$ reaches its maximum and minimum, respectively. This yields a preliminary ν that is rounded off to the nearest integer. The combination of ν and $t_{p,\min} - t_{p,\max}$ yields the pulse's t_r. The signature is time-shifted by t_{sh} to align its zero-crossing with that of $p(t)$, and the pulse amplitude is assigned. The resulting ∂_tWP, with its parameters, is shown in Fig. 7. The deviation with respect to $p(t)$ is

$$\mathrm{Err}(p) = \frac{\int_{t=0\,\mathrm{ps}}^{500\,\mathrm{ps}} \left[p(t) - \partial_t \mathrm{WP}(t)\right]^2 \mathrm{d}t}{\int_{t=0\,\mathrm{ps}}^{500\,\mathrm{ps}} p^2(t) \mathrm{d}t} = 0.08\,(\%) \qquad (13)$$

a practically perfect replication! The circuitry for generating WP monocycles can then be deemed as readily available.

VI. Conclusion

A novel family of model pulses was constructed from a WP unipolar prototype. The prototype and its time-derivatives have finite temporal support and are continuous at onset and end up to controlled differentiation orders. The prototype's shape is tailored via two parameters only. As a time-windowing function, its SpL is below -46 dB. A WP monocycle was derived by time-differentiating the prototype. Practical rules for its design were given. The family was supplemented with the WP modulated–sinc–cosine pulse featuring an almost rectangular spectral diagram and lower than -60-dB SpL levels. The WP monocycle was shown to be extremely effective as excitation in EM analyses: time-windowed simulations using it yielded up to 31.5 times lower computation times when compared to standard excitations, while ensuring identical accuracy. This pulse's signature was also shown to be reproducible via readily available circuitry. This recommends the WP family of pulses for excitation in computational EM, for time-windowing purposes, and as feeding signals for pulsed-field or timed antenna systems.

Acknowledgment

The authors would like to thank Prof. T. Kikkawa of the Hiroshima University, Japan, for granting the permission to reproduce the signal signature in [11, Fig. 10(b)].

References

[1] I. E. Lager, A. T. de Hoop, and T. Kikkawa, "Model pulses for performance prediction of digital microelectronic systems," *IEEE Trans. Compon., Packag., Manuf. Technol.*, vol. 2, no. 11, pp. 1859–1870, Nov. 2012.

[2] I. E. Lager and A. T. de Hoop, "Causal pulses with rectangular spectral content: A tool for TD analysis of UWB antenna performance," *IEEE Antennas Wireless Propag. Lett.*, vol. 12, pp. 1488–1491, 2013.

[3] J. J. Knab, "Interpolation of band-limited functions using the approximate prolate series," *IEEE Trans. Inf. Theory*, vol. IT-25, no. 6, pp. 717–720, Nov. 1979.

[4] G. Franceschetti, J. Tatoian, and G. Gibbs, "Timed arrays in a nutshell," *IEEE Trans. Antennas Propag.*, vol. 53, no. 12, pp. 4073–4082, Dec. 2005.

[5] W. Wiesbeck, G. Adamiuk, and C. Sturm, "Basic properties and design principles of UWB antennas," *Proc. IEEE*, vol. 97, no. 2, pp. 372–385, Feb. 2009.

[6] I. E. Lager and A. T. de Hoop, "Loop-to-loop pulsed electromagnetic field wireless signal transfer," in *Proc. 6th Eur. Conf. Antennas Propag.*, 2012, pp. 786–790.

[7] E. W. Weisstein, *CRC Concise Encyclopedia of Mathematics*. Boca Raton, FL, USA: CRC Press, 1999.

[8] I. E. Lager, S. L. van Berkel, N. Llombart-Juan, and A. Neto, "Time-domain EM numerical modelling: A pulse shape causality and temporal support analysis," in *Proc. 10th Eur. Conf. Antennas Propag.*, 2016, pp. 1–5.

[9] M. Abramowitz and I. A. Stegun, *Handbook of Mathematical Functions*. Mineola, NY, USA: Dover, 1968.

[10] F. Mesa, C. di Nallo, and D. R. Jackson, "The theory of surface-wave and space-wave leaky-mode excitation on microstrip lines," *IEEE Trans. Microw. Theory Techn.*, vol. 47, no. 2, pp. 207–215, Feb. 1999.

[11] M. Hafiz, S. Kubota, N. Sasaki, K. Kimoto, and T. Kikkawa, "A 2 Gb/s 1.8 pJ/bit differential BPSK UWB-IR transmitter using 65 nm CMOS technology," *IEICE Trans. Electron.*, vol. E94-C, no. 2, pp. 977–984, Feb. 2011.